15TH IEA HEAT PUMP CONFERENCE
MAY 26–29, 2026 | HOFBURG
VIENNA 2026
DECARBONISATION THROUGH INNOVATION

Exergetic and energetic comparison of reverse Rankine, Brayton, and Stirling heat pump cycles for district heating applications

Verena Jetzinger[a,b,*], Matthias Finkenrath[a], Miguel Gonzalez-Salazar[b]

[a]Kempten University of Applied Sciences, Bahnhofstraße 61, 87435 Kempten, Germany
[b]Technical University of Applied Sciences Würzburg-Schweinfurt, Ignaz-Schön-Straße 12, 97421 Schweinfurt, Germany

Abstract

Integrating heat pumps into district heating systems is a key strategy for increasing the share of renewable energies in the heating sector, especially in urban areas. Yet, district heating networks are diverse, often posing significant challenges on heat pumps. This study provides a potential analysis of three fundamental heat pump cycles – vapor compression, reverse Brayton, and reverse Stirling – with a focus on district heating applications by conducting a comprehensive exergetic and energetic comparison. For this purpose, both ideal and non-ideal process models are applied to capture thermodynamic potentials and the impact of key loss factors under typical district heating conditions. The coefficient of performance (COP) serves as an indicator of energetic efficiency, while exergy loss quantifies the integration quality of the processes into district heating systems. The results demonstrate that the reverse Brayton heat pump constitutes the theoretical optimum under idealized assumptions, achieving the highest COPs and lowest exergy losses. However, once non-ideal effects are introduced, this advantage diminishes substantially. Under realistic conditions, the vapor compression heat pump delivers the highest COPs and proves most robust with respect to loss factors such as pressure drops and isentropic efficiency. The reverse Brayton heat pump shows strong dependence on very high isentropic efficiencies in compression and expansion stages, which poses a major challenge for practical application. The reverse Stirling heat pump consistently occupies an intermediate position in context of efficiency, exergy losses and sensitivity to loss factors. By abstracting from specific technologies, this study delivers a comprehensive evaluation of the three cycles in district heating, highlighting their thermodynamical capability.

Selection and/or peer-review under the responsibility of the organizers of the 15th IEA Heat Pump Conference 2026.

Keywords: Thermodynamic comparison; exergy loss analysis; fundamental process analysis; reverse Rankine cycle; reverse Brayton cycle; reverse Stirling cycle; district heating applications

1. Introduction

Decarbonization of the heating sector represents one of the central challenges on the path towards climate neutrality. Heating and cooling accounts for about 50 % of the final energy consumption in Europe [1]; however, only 26.2 % originated from renewable energy sources in 2023 [1, 2]. District heating (DH) has the potential to offer a sustainable heat supply when integrated with renewable heat sources, especially in urban areas, and is expected to expand significantly in the coming years. In this context, heat pumps (HP) have emerged as a central technology to integrate low-temperature renewable heat sources or waste heat into DH networks. With a share of only 1.9 % in Europe in 2022, HPs in DH show strong growth potential [3]. However, the integration of HPs into DH networks poses special challenges. Firstly, DH networks require flexible operation across varying temperature levels on both heat source and sink sides. Furthermore, many networks operate at very high supply temperatures of 130 °C or above [4], even though there are increasing efforts to

* Corresponding author. Tel.: +49 (0) 831-2523-9313
E-mail address: verena.jetzinger@hs-kempten.de

decrease DH supply temperatures for higher efficiency and facilitated integration of renewable energies. At the same time, many heat sources are available only at low temperatures, especially during cold months. The high temperature lift can become challenging with regard to technical feasibility and efficiency. Consequently, there is a need to explore HP solutions that can operate efficiently under variable network conditions.

Market overviews such as in [5–7] show that the vast majority of HP technology consists of electrically or mechanically driven closed-loop HPs. The vapor compression heat pump (VCHP) is by far the most widely deployed HP technology today. Nevertheless, the reverse Brayton heat pump (BHP) and the reverse Stirling heat pump (SHP) are being continuously developed and are already commercially available [8–10]. For all three types, a refrigerant circulates in a closed loop and undergoes four state changes: Compression, heat rejection, expansion and heat absorption. Yet, the cycles bear several differences in process paths. Firstly, the refrigerant of the VCHP experiences phase changes during the heat absorption and rejection, whereas process fluids of BHP and SHP cycles remain solely gaseous. Furthermore, the heat rejection and absorption process is directly linked to the heat source and sink for the VCHP and BHP; meanwhile these state changes happen internally for the SHP. The external heat exchange occurs during the compression and expansion. Another key difference is that VCHP and BHP can account as steady-state flow processes, whereas the state variables change continuously in the working space of the SHP during the cycle.

Both the BHP and SHP concepts can show advantages, particularly when operating with cold heat sources or hot heat sinks, where the technical feasibility of VCHPs is limited by the properties of the refrigerant. BHP and SHP also benefit from the use of environmentally benign working fluids, such as air or noble gases. Although natural refrigerants are also available for VCHPs, their operating temperature range is constrained by the phase-change mechanism. Another key driver for alternative HP cycles is their improved part-load behavior [11]. BHPs have been shown to reach comparable or superior coefficients of performance (COP) to VCHPs, particularly at low source and high sink temperatures [12–14]. However, outperforming VCHPs requires highly efficient compression and expansion, identified at 95 and 96 % [14–16]. In rotation heat pumps (RHP) such as [8], which are an innovative derivative of the BHP, the pressure rise is generated by centrifugal forces, leading to very high isentropic efficiencies. For this technology, efficiencies above 99 % can be achieved [14]. Compared to VCHPs, SHP are particularly attractive for applications involving very high sink temperatures [9] or very low source temperatures [17, 18]. Ref. [18] compares a SHP with different VCHP systems for domestic heating in cold regions and conclude that SHPs can achieve equal or even higher COPs than VCHPs under such conditions.

Existing literature primarily provides plant-specific comparisons, while fundamental cycle characteristics remain largely unaddressed. Furthermore, the comparison between the three basic processes is missing. This lack of fundamental insights limits the ability to derive generalizable conclusions on the comparative performance and optimal operating conditions of the different cycles. Moreover, the literature demonstrates that inefficiencies and operating conditions critically determine which technology is best suited [13, 15, 16, 18]. However, no systematic analysis exists regarding the role of individual loss factors and the conditions under which these processes can achieve comparable efficiencies.

This study offers a systematic and consistent thermodynamic comparison of the fundamental processes of VCHP, BHP and SHP. The study deliberately avoids the consideration of plant-specific technological implementations to reach optimum comparability between the cycles. It hereby focuses specifically on DH applications with respective temperature levels and glides. Firstly, a theoretical comparison is performed based on ideal cycle assumptions in order to highlight the thermodynamic optimum. Secondly, inefficiencies are considered, leading to a more realistic comparison. Using the comparison, a sensitivity analysis of the relevant loss mechanisms is performed to identify the performance requirements for the processes needed to reach comparable efficiencies. This work is therefore conceived as a potential analysis of the fundamental cycles.

2. Heat pump model assumptions and system integration

2.1. Heat pump loss mechanisms

For VCHPs and BHPs, the main inefficiencies arise from non-ideal compression and expansion, as well as pressure losses in the heat exchangers (HX).

For the VCHP, pressure drop in HXs is neglected in many studies [19, 20]. Ref. [21] has observed pressure drops between approximately 10 and 60 kPa in the condenser and between approximately 5 and 15 kPa in the evaporator, dependent on the refrigerant mass flow. Isentropic efficiencies depend on the compressor type. Typical values range from approximately 70 % for rotary vane and 75 % for scroll and piston up to 85 % for centrifugal turbo compressors [22, 23].

The efficiency of BHPs is known to be sensitive to pressure losses [24]. However, the way they are considered differs substantially across studies. While Ref. [25] assumes no pressure losses, Ref. [26] observes a pressure loss range between 0 and 100 kPa per HX and estimates it constant at 20 kPa for both hot-side heat exchanger (HHX) and cold-side heat exchanger (CHX) for specific studies. Ref. [12] refers to a physical single-phase pressure loss model presented by [27]. Ref. [24] introduces a fractional pressure loss factor. The overall factor, which can be approximated as the sum of the individual pressure loss factors for small values, is observed in a range from 0 to 5 %. Irreversible effects during compression and expansion are taken account for by the isentropic efficiency. Studies show high potential values between 80 and 93 % for the compressor and between 80 and 95 % for the expander [11, 16, 28, 29]. The efficiency of BHP also depends on the operating pressure with typical lower pressure levels of between 220 and 270 kPa [26, 30].

When describing a non-ideal SHP thermodynamically, the main challenge is to capture its transient cycle behaviour and central loss mechanisms holistically, but with comparable level of detail to VCHP or BHP models. Ref. [31] provides a comprehensive overview of modeling approaches for Stirling engines, revealing that a wide range of loss factors exists and that their representation is often highly machine-specific. Moreover, the modeling approach can become arbitrarily complex once departing from an ideal and simplified analysis. The Finite Speed Thermodynamics (FSDT) approach, introduced in Ref. [32] and discussed in detail in Ref. [33], addresses this by accounting for irreversibilities arising from finite operating speeds, as it is the case for the SHP. The derived direct method allows analytical efficiency determination based on a novel formulation of the first law of thermodynamics and has been widely applied to Stirling cycles [34–36], particularly for optimization. Ref. [37] adapts this method for SHPs to calculate the COP while including pressure and regenerator losses. Pressure losses are typically modelled as functions of temperature, pressure, working fluid and frequency, considering fluid and mechanical friction as well as piston speed [35–38]. Regenerator efficiency, usually between 80 and 90 % [39–41], quantifies the effectiveness of heat recovery.

2.2. System integration

This study places its focus especially on the integration of HPs into DH applications. The heat sink corresponds to the DH network with the return flow equaling the heat sink inlet and the supply flow corresponding to the heat sink outlet. Typical DH networks can be categorized into five generations, each depending amongst other factors on type of heat generation, supply and return flow temperature as shown in Table 1. This study focuses on DH networks of 2nd, 3rd and 4th generation.

Table 1. Overview of district heating generations based on [32–34].

	1st generation	2nd generation	3rd generation	4th generation	5th generation
Heat carrier	Steam	Hot water	Hot water	Water	Cold water
Supply temperature	< 200 °C	> 100 °C	< 100 °C	50 – 60 °C (70 °C)	Close to ground temperature
Return temperature	< 80 °C	< 70 °C	< 45 °C	< 25 °C	Close to ground temperature

An overview of possible heat sources is presented by Ref. [35]. Ambient air exhibits seasonal variations between -20 and 40 °C, surface water temperatures typically range from -1 to 25 °C and groundwater and mine water typically remain within a narrow band of 10 to 12 °C [35]. Across the HXs, temperature gradients between 5 and 10 K are plausible [36]. Near-surface geothermal sources vary with depth, showing 0 to 17 °C at the surface and stabilizing at around 10 °C below depths of 15 m [37]. Industrial heat sources typically range from 10 to above 100 °C [35]. Sewage water exhibits a mean temperature of 13.1 °C and seasonal variations from 8.4 to 18.2 °C [38]. Associated temperature gradients are typically 3 to 6 K [7, 39].

3. Methodology

3.1. Comparison metrics

This study uses two key metrics to compare the processes and evaluate their suitability for DH applications. Firstly, the COP serves as an indicator of HP energy efficiency. Secondly, the exergy loss of the processes is analyzed to assess system integration quality. Thus, the evaluation reflects both thermodynamic performance and the integration potential in DH networks.

3.1.1. Coefficient of performance (COP)

The COP is a dimensionless metric to evaluate the energy efficiency of a HP system and compares the energetic benefit to the energetic input. It is defined as the ratio of externally rejected heat $\dot{Q}_{rejected}$ to the net input power P_{net} as shown in Eq. (1). The net input power corresponds to the difference between compression power P_{compr} and expansion power P_{exp}, if expansion work is used.

$$\mathrm{COP} = \frac{|\dot{Q}_{rejected}|}{P_{net}} = \frac{|\dot{Q}_{rejected}|}{P_{compr} - |P_{exp}|} \tag{1}$$

In case of ideal process operation, the energy efficiency can be expressed as Carnot or Lorenz COP, representing the maximum achievable COP. The Carnot COP applies to isothermal heat exchange, whereas the Lorenz COP accounts for temperature glide during heat absorption or rejection [40].

3.1.2. Exergy loss

Exergy loss is a common metric to describe the irreversibilities within a thermodynamic process, which is useful for identifying potential improvements. Especially in the field of integrating HPs into existing systems, the indicator is widely used to assess the quality of their incorporation into an overall system. To quantify the exergy loss in an HX, the exergy content of both hot and cold side, ex_{hot} and ex_{cold}, is evaluated. The exergy loss Δex_{loss} is then obtained as the difference between the exergy contents as shown in Eq. (2). The equation shows furthermore, that the exergy loss increases for higher deviations between T_{cold} and T_{hot}.

$$\Delta ex_{loss} = ex_{hot} - ex_{cold} = \int_0^q \left(\frac{T_0}{T_{cold}(q)} - \frac{T_0}{T_{hot}(q)}\right) dq \tag{2}$$

The integration points of the HP into the system are defined by CHX and HHX. To evaluate system integration quality, the total exergy loss $\Delta ex_{loss,total}$ considered in this study results from the external heat transfer in only these two components and is determined using Eq. (3).

$$\Delta \mathrm{ex}_{\mathrm{loss,total}} = \Delta \mathrm{ex}_{\mathrm{loss,CHX}} + \Delta \mathrm{ex}_{\mathrm{loss,HHX}} \tag{3}$$

3.2. Ideal process models

For an idealized observation, the refrigerants of VCHP, BHP and SHP undergo four state changes during one cycle as shown in Table 2: Compression, heat rejection, expansion and heat absorption. Furthermore, ideal gas properties are assumed for the ideal process models.

Table 2. Idealized state changes of VCHP, BHP and SHP.

	Ideal VCHP	**Ideal BHP**	**Ideal SHP**
1 → 2 (Compression)	Isentropic	Isentropic	Isothermal (Heat rejection to ambient)
2 → 3 (Heat rejection)	Isobaric (with phase change)	Isobaric	Isochoric (Internal heat exchange)
3 → 4 (Expansion)	Isentropic (Isenthalpic)	Isentropic	Isothermal (Heat absorption from ambient)
4 → 1 (Heat absorption)	Isobaric (with phase change)	Isobaric	Isochoric (Internal heat exchange)

In this study, the ideal reverse Rankine cycle forms the basis of the idealized VCHP model. Although the Rankine cycle expands the working fluid isentropically in a turbine, whereas HPs usually use an isenthalpic throttling process [41], an isentropic expansion is assumed here to estimate the maximum efficiency of technically realizable cycles. Thus, approximating the reverse Rankine cycle for the VCHP is justified. Furthermore, it is assumed that the refrigerant is superheated by 5 K after compression, consistent with real-world applications. Additionally, the heat required for the superheating is assumed to account for 5 % of the total heat output of the cycle. When not taking superheating into consideration, the ideal COP corresponds to the Carnot COP. However, determining the ideal COP with superheating bears the difficulty that the rejected heat is partly latent, partly sensitive. Thus, neither the Carnot COP nor the Lorenz COP is solely accurate in this case. Therefore, the COP is weighted according to the respective share of rejected heat.

In the ideal BHP, a minimum temperature pinch of 5 K is ensured. To achieve this, the refrigerant temperature profile is aligned with the side of the heat transfer process (source or sink) exhibiting the higher temperature gradient. In the present study, this corresponds to the heat sink side, where only an upper terminal temperature difference (TTD) is defined for the CHX. To determine the missing temperature, the ideal gas relation for isentropic compression and expansion shown in Eq. (4) is applied. Assuming isobaric heat transfer and ideal gas properties, the temperature correlation can be expressed as in Eq. (5). The COP of the ideal reverse Brayton cycle corresponds to the Lorenz COP. The indices in all following equations correspond to the states listed in Table 2.

$$\frac{T_2}{T_1} = \left(\frac{p_2}{p_1}\right)^{\frac{\kappa-1}{\kappa}} \text{ and } \frac{T_3}{T_4} = \left(\frac{p_3}{p_4}\right)^{\frac{\kappa-1}{\kappa}} \tag{4}$$

$$\frac{T_2}{T_1} = \frac{T_3}{T_4} \tag{5}$$

For the ideal reverse Stirling cycle, the external heat exchange takes place during the isothermal compression and expansion. The COP of the ideal reverse Stirling cycle corresponds to the Carnot COP.

3.3. Non-ideal process models

The VCHP model consists of a compressor, a HHX, a valve and a CHX in sequence. Key design parameters include the heat sink and source temperatures at the inlet and outlet of the respective HX, the isentropic compressor efficiency and pressure losses. Other considerations include: The compression is forced to end in the superheated area and the fluid expands isenthalpically in the valve. The model accounts for irreversibilities of the compressor due to non-isentropic compression and pressure drops in CHX and HHX. Since the vapor compression HP expands via a valve instead of a turbine, no expansion work is performed. Therefore, the net input power equals the compressor power. The COP is calculated using Eq. (6).

$$\mathrm{COP_{VCHP}} = \frac{|\dot{Q}_{rejected}|}{\mathrm{P_{comp}}} = \frac{|\mathrm{h_3 - h_2}|}{\mathrm{h_2 - h_1}} \tag{6}$$

In contrast to the VCHP model, the BHP expands via a turbine instead of a valve. The system layout, comprising a compressor, HHX, turbine and CHX, follows a similar component order and the HP also operates in steady-state. Key inefficiencies arise from pressure drops in the CHX and HHX and from the non-isentropic behavior of compressor and turbine, in analogy to the VCHP. The COP of the BHP is calculated according to Eq. (7). The model adapts so that the heat capacity flows on both the HP and heat sink side are identical.

$$COP_{BHP} = \frac{|\dot{Q}_{rejected}|}{P_{comp} - |P_{exp}|} = \frac{|h_3 - h_2|}{(h_2 - h_1) - |(h_4 - h_3)|} \tag{7}$$

For the SHP, the FSDT method is applied. Firstly, energy flows are calculated according to the ideal state changes given in Table 2. The transferred heat flows are calculated according to Eq. (8) with fluid properties from REFPROP [42]. The reversible net input work is determined as given in Eq. (9). The COP is then determined using Eq. (10) [43]. The usable heat Q_{12} is reduced by the heat that cannot be regenerated. The net input work on the other hand is increased by the additional work W_{loss} needed to overcome pressure losses. Lastly, it is assumed that a specific share y of the additional work is converted into usable heat.

$$Q = m \cdot T \cdot \Delta s \tag{8}$$

$$W_{net} = Q_{12} - Q_{34} \tag{9}$$

$$\mathrm{COP_{SHP}} = \frac{\mathrm{Q}}{\mathrm{W}} = \frac{\mathrm{Q_{12}} - (1 - \eta_{\mathrm{reg}}) \cdot \mathrm{Q_{23}} + \mathrm{y} \cdot \mathrm{W_{loss}}}{\mathrm{W_{net}} + \mathrm{W_{loss}}} \tag{10}$$

3.4. Model and temperature assumptions

Table 3 gives an overview of the chosen model parameters. HXs are assumed to operate counter-currently. A pinch of 5 K is ensured in all HXs. Additionally, for the BHP, a lower pressure level of 250 kPa is assumed.

Table 3. Parameters and assumptions for ideal and non-ideal HP models.

Process	Pinch	$\eta_{s,comp}$	$\eta_{s,exp}$	η_{reg}	Δp_{loss}	Specification of TTD (= 5 K)
VCHP (ideal)	5 K	1	1	-	0	Evaporator (CHX): Lower TTD; Condenser (HHX): None (Pinch)
VCHP	5 K	0.85	-	-	2.5 % of operating pressure per HX	Evaporator (CHX): Lower TTD; Condenser (HHX): Upper and lower TTD
BHP (ideal)	5 K	1	1	-	0	HHX: Upper and lower TTD; CHX: Upper TTD
BHP	5 K	0.85	0.85	-	2.5 % of operating pressure per HX	HHX: Lower TTD; CHX: Upper TTD
SHP (ideal)	5 K	-	-	1	0	HHX: Upper TTD; CHX: Lower TTD
SHP	5 K	-	-	0.85	Estimated via [44]	HHX: Upper TTD; CHX: Lower TTD

For the temperature levels, conditions as typical as possible faced by HPs in DH networks are applied. Table 1 shows, that typical temperature differences between supply and return flow are between 30 and 55 °C for DH networks of 2nd, 3rd and 4th generation. Therefore, a constant temperature glide of 35 °C is assumed. The investigated supply temperatures range from 60 to 110 °C. Temperature levels in heat sources can vary depending on the type of heat source as well as on weather conditions, daytime or season. Temperature glides however appear to be similar for most environmental heat sources, usually amounting to a few Kelvin. Thus, a heat source temperature of 10 °C is applied, with a 5 K temperature glide in the HX. The choice of refrigerant for the VCHP is limited by the high temperature lift and the operating temperature range. Ammonia, a natural, low-impact refrigerant, is identified as suitable with a possible operating temperature range of around -30 to 110 °C [6]. For the BHP and SHP, the common working fluids air and helium are employed.

4. Results and discussion

4.1. Process comparison

When comparing ideal processes for typical DH application as in Fig. 1a, the BHP offers the highest theoretical potential for an efficient integration. VCHP and SHP show lower COPs, yet yield similar results, with the VCHP exhibiting a slightly higher performance. The difference results from the superheating of the VCHP. If the cycle was assumed with no superheating, both the ideal VCHP and SHP cycles would correspond to the reverse Carnot cycle, offering an identical Carnot COP.

For the non-ideal processes, results differ significantly: Although the ideal BHP offers the highest potential in theory, it performs worst when real-life effects are considered (see Fig. 1b). On the contrary, the VCHP provides the highest COPs for the observed supply temperature range, with the SHP lying in between. The figure shows furthermore, that the VCHP is most sensitive to variation of the supply temperature. The COP of SHP is more stable and the BHP operates nearly COP-neutral for supply temperatures of 85 °C and above.

Fig. 2 compares the total exergy losses in the CHX and HHX of the three ideal HP processes shown in (a) and further analyzes them distributed to the CHX and HHX in (b) and (c). In terms of total exergy losses, the BHP exhibits the lowest values, meaning that the BHP shows the overall best theoretical system integration quality. The VCHP and SHP experience higher exergy losses, with the SHP reaching maximum values. In general, exergy losses decrease with higher supply temperatures if the transferred heat is identical (see Eq. 2).

In the CHX, the exergy losses of VCHP and SHP are identical. This results from the isothermal nature of the heat transfer: in the case of the VCHP due to latent heat exchange during evaporation, and in the case of the SHP, due to external heat absorption during isothermal expansion. Figure 2b further shows that the exergy loss decreases at higher supply temperatures. For the VCHP and SHP, this is due to a reduction in the COP at higher supply temperatures. While the same amount of heat is rejected to the sink, the heat absorbed by the system decreases. According to the calculation in Eq. 2, this results in a lower exergy loss. For the BHP, two effects come together: Firstly, the COP decreases with increasing supply temperature as well, meaning that the absorbed heat from the heat source decreases here, too. Secondly, the effect described in Eq. 5 becomes relevant. Here, T_1 remains constant, but T_2 and T_3 increase while maintaining a constant temperature difference them. As a result, T_4 increases too, leading to a decrease in exergy loss. In general, the exergy loss of the BHP is higher in the CHX than that of the VCHP and SHP. This results from the high discrepancy of temperature gradients of refrigerant and heat source detailed in Section 3.4. The isothermal heat absorption of VCHP and SHP matches the temperature glide significantly better.

In the HHX, the BHP shows the lowest exergy losses due to the identical temperature gradient resulting from equal heat capacity flows in the HHX. The remaining exergy destruction is therefore only caused by the pinch. For the VCHP and SHP, exergy losses in the HHX are significantly higher than in the CHX as a result of the difference in temperature gradient between refrigerant and heat sink side (see assumptions Section 3.4). The exergy loss of the VCHP is yet lower as a result of the additional temperature gradient introduced by superheating. The exergy loss decreases with the higher supply temperature in the HHX as well. This results from the definition in Eq. (2). At a constant reference temperature T_0, the exergy loss decreases at higher temperatures T_{cold} and T_{hot}.

It can be concluded that the exergy losses of the BHP primarily originate from the CHX, whereas the VCHP and SHP exhibit their main inefficiencies in the HHX. Consequently, these components represent the critical interfaces for system integration. All in all, the BHP shows the best theoretical system integration quality.

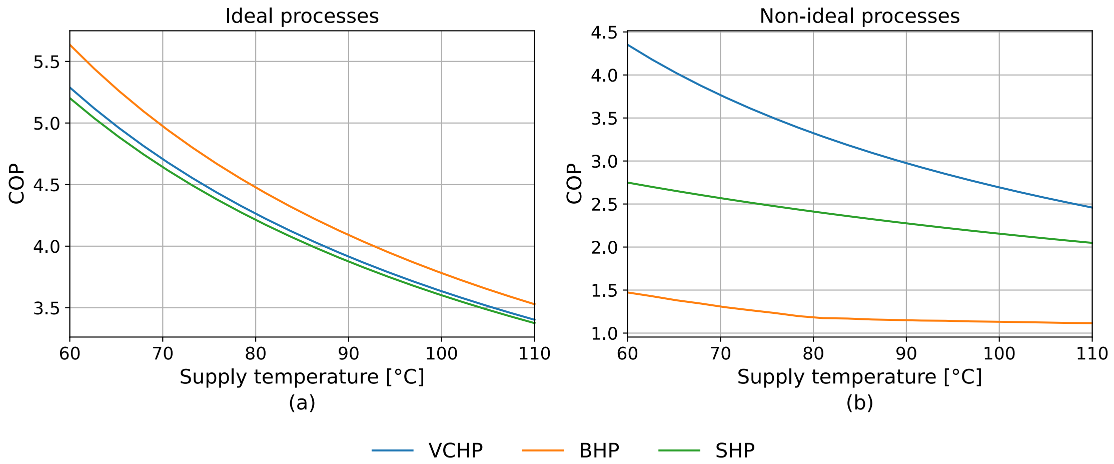

Figure 1. Comparison of COP for VCHP, BHP and SHP as (a) ideal and (b) non-ideal processes.

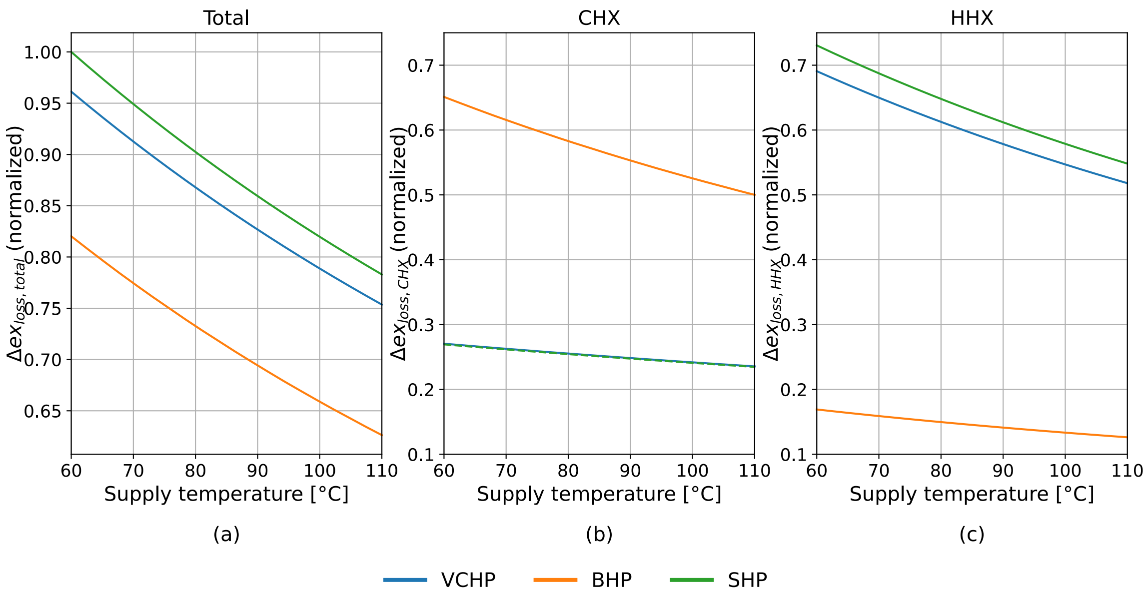

Figure 2. Exergy losses of ideal cycles: (a) total exergy loss in CHX and HHX, (b) distribution in CHX and (c) distribution in HHX.

4.2. Sensitivity to loss factors

As shown before, loss factors can have an essential impact on real-world HP applications. Fig. 3 shows the effect of the respective inefficiencies on the behavior of VCHP, BHP and SHP for different supply temperatures. For VCHP, the isentropic efficiency of the compression produces the main inefficiency, while pressure losses have a marginal impact on HP efficiency. The influence of both factors decreases at higher supply temperatures. The BHP is also mainly influenced by the isentropic efficiency of the compressor and turbine. However, the effect of pressure losses has significantly more impact on the BHP than on the VCHP. For the SHP, pressure losses have the largest impact on the COP. However, by recovering heat resulting from dissipation due to pressure losses, the loss in efficiency can be mitigated. It must be noted, that pressure losses in case of the SHP are not caused by HX hydraulics as in case of the VCHP and SHP, but by different effects, such as internal friction of the fluid, mechanical friction of the piston, as well as the piston speed. Furthermore, although not as significant as pressure losses, the regenerator efficiency also has a non-negligible impact on the efficiency of the SHP. In general, the BHP shows the highest sensitivity to inefficiencies, whereas the VCHP is only moderately affected. In contrast, the VCHP is the most sensitive to variations in the supply temperature, whereas the BHP provides a more robust performance in this context.

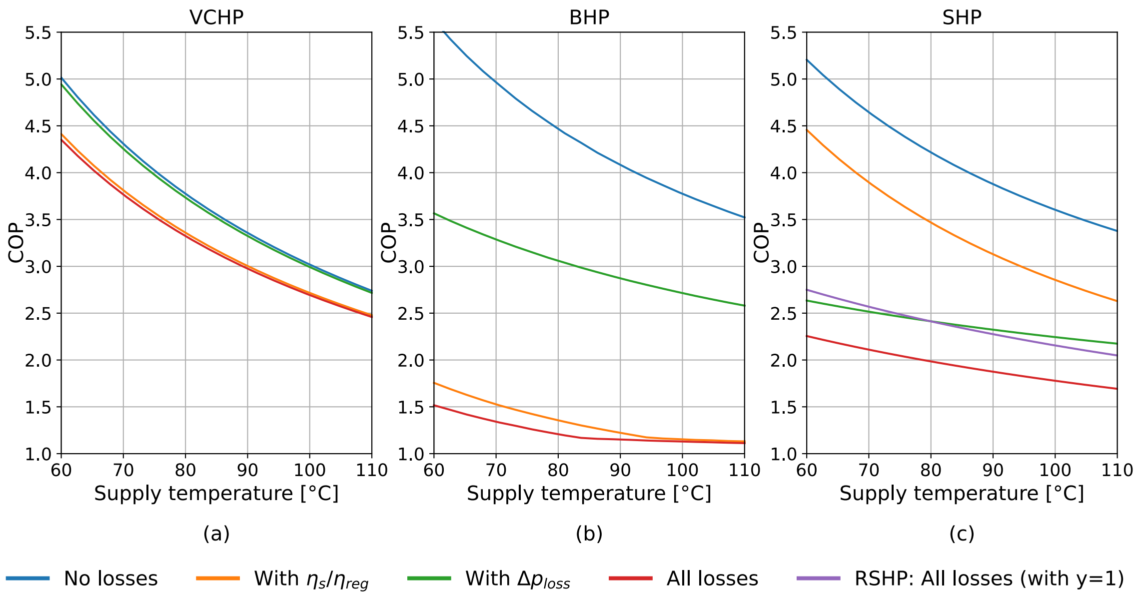

Figure 3. Impact of different inefficiencies on COP for (a) VCHP, (b) BHP and (c) SHP at varying supply temperatures.

The assumptions about the impact of the loss factors are confirmed and extended by a sensitivity analysis in Fig. 4. The reference supply temperature is 90 °C. The previously described behavior of the VCHP showing little sensitivity to pressure losses can also be seen in Fig. 4a. While isentropic efficiency is the parameter that influences the COP of the VCHP most, the impact is relatively small compared to BHP and SHP. The BHP in (b) shows the largest range of possible COPs, with both the highest and lowest COPs of all three processes, highly dependent on the isentropic efficiency. Unlike the VCHP and SHP, the COP of the BHP exhibits a pronounced convex dependence on the isentropic efficiency, indicating an accelerated increase in COP at higher isentropic efficiencies. Furthermore, the influence of pressure losses cannot be neglected for the BHP, especially at high isentropic efficiencies. The SHP in (c) proves to be highly sensitive to both regenerator efficiency and pressure losses. The comparison illustrates that the VCHP is the most robust technology, offering the smallest variation in COP against loss factors. In contrast, the BHP is highly sensitive to the isentropic efficiency of compression and expansion, requiring values that cannot be achieved with conventional compression and expansion. However, RHPs claim to be able to reach necessary values and therefore outperform VCHPs [14]. In general, the findings demonstrate that while the VCHP offers the highest robustness under varying losses, BHPs and SHPs require optimized efficiencies and pressure losses to fully exploit their thermodynamic potential.

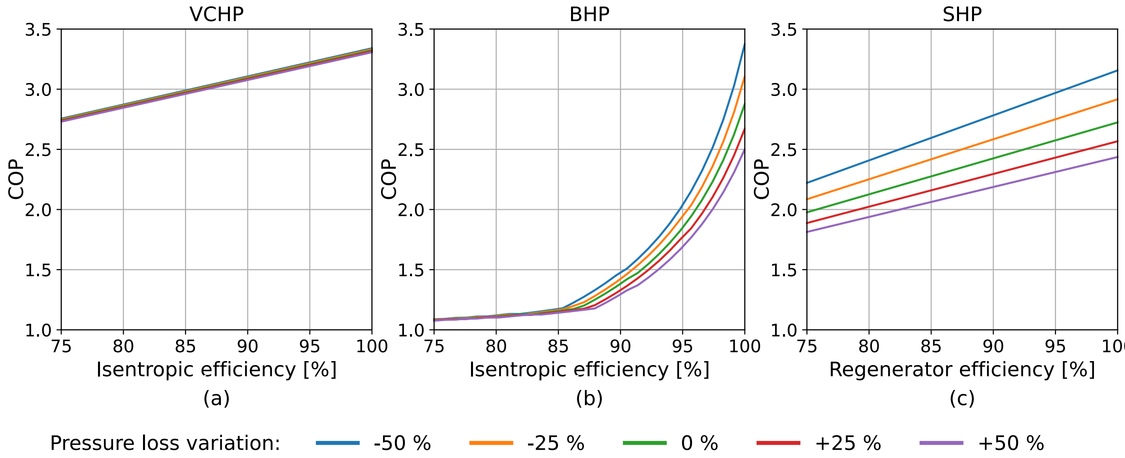

Figure 4. Sensitivity of COP to pressure losses and efficiencies for (a) VCHP, (b) BHP and (c) SHP at 90 °C supply temperature.

5. Conclusion

In this study, the three main basic processes of closed-loop mechanically driven HPs have been analyzed and compared with regard to specific DH temperature requirements. Both ideal and non-ideal cycles have been investigated considering COP and exergy loss as metrics to evaluate efficiency and system integration quality. The key findings allow the following conclusions to be drawn:

(1) The BHP represents the theoretical optimum for the investigated DH applications in terms of both efficiency and system integration quality.
(2) The VCHP achieves the highest COPs with current state-of-the-art technology. Nevertheless, the BHP could become technologically competitive if very high isentropic efficiencies (such as reported for the RHP) can be achieved.
(3) The VCHP is the most robust to inefficiencies but the most sensitive to supply temperature variations, whereas the BHP is highly affected by isentropic efficiency.
(4) The SHP occupies the mid-range of the three technologies in terms of ideal and non-ideal efficiency, system integration quality and sensitivity to efficiency and supply temperature.

However, this study has placed its focus on basic HP processes and estimated their potential for DH applications. For a holistic evaluation, future work needs to take further plant and operation properties into account, such as efficiency-enhancing components and fluids, part-load behavior or economic and environmental aspects, as well as more sophisticated process designs.

Nomenclature

ex	Specific exergy [J/kg]	$\dot{Q}$	Thermal power [W]
h	Specific enthalpy [J/kg]	s	Specific entropy [J/kg/K]
m	Mass [kg]	T	Temperature [K]
p	Pressure [Pa]	W	Work [J]
P	Power [W]	y	Share of recovered heat [-]
q	Specific heat [J/kg]	η	Efficiency [-]
Q	Heat [J]	κ	Isentropic exponent [-]

Acknowledgements

This work was funded by the German Federal Ministry for Economic Affairs and Climate Action under the funding codes 03EN3073 and 03EN3107B, with additional financial and in kind support from the project partners AGFW, Fernwärme Ulm GmbH, ZAK Energie GmbH, Stadtwerke Schweinfurt GmbH, ecop Technologies GmbH and Siemens Energy GmbH & Co. KG. The responsibility for the content of this publication lies with the authors.

References

[1] Heat Roadmap Europe, *Heating and Cooling: Facts and Figures. The Transformation towards a Low-Carbon Heating & Cooling Sector.* [Online]. Available: https://heatroadmap.eu/wp-content/uploads/2019/03/Brochure_Heating-and-Cool.pdf

[2] Eurostat, "Renewable energy statistics," 2025. [Online]. Available: https://ec.europa.eu/eurostat/statistics-explained/index.php?title=Renewable_energy_statistics

[3] Euroheat & Power, "DHC Market Outlook," 2024. [Online]. Available: https://www.euroheat.org/data-insights/outlooks/dhc-market-outlook-2024

[4] AGFW e.V., *AGFW Hauptbericht 2023*.

[5] B. Zühlsdorf *et al.,* "IEA HPT Annex 58: High-Temperature Heat Pumps. Task 1 Report: Technologies," Heat Pump Centre c/o RISE – Research Institutes of Sweden, 2023. [Online]. Available: https://heatpumpingtechnologies.org/annex58/wp-content/uploads/sites/70/2023/09/annex-58-task-1-technologies-task-report.pdf

[6] C. Arpagaus, "Hochtemperatur-Wärmepumpen," *Marktübersicht, Stand der Technik und Anwendungspotenziale. Berlin, Offenbach: VDE Verlag GmbH*, 2019.

[7] AGORA Energiewende and IEG Fraunhofer, "Roll-out von Großwärmepumpen in Deutschland," *Strategien für den Markthochlauf in Wärmenetzen und Industrie*, 2023.

[8] ecop Technologies GmbH, "Rotation Heat Pump – Industrial High-Temperature Heat Pump Technology," 2025. [Online]. Available: https://www.ecop.at/en/home-4/

[9] Tetra Pak International S.A., *Tetra Pak HighLift Heat Pump by Olvondo Technology™: Product Leaflet.* [Online]. Available: https://www.tetrapak.com/content/dam/tetrapak/media-box/global/en/documents/tetra-pak-highlift-heat-pump-pd-leaflet.pdf

[10] Enerin AS, "HoegTemp – Ultra High-Temperature Heat Pumps," 2025. [Online]. Available: https://www.enerin.no/hoegtemp

[11] C.-L. Zhang and H. Yuan, "An important feature of air heat pump cycle: Heating capacity in line with heating load," *Energy*, vol. 72, pp. 405–413, 2014.

[12] J.-S. Kim, I.-H. Chung, T.-S. Kim, and C.-H. Song, "Thermal Performance Design and Analysis of Reversed Brayton Cycle Heat Pumps for High-Temperature Heat Supply," *Energies*, vol. 17, no. 12, p. 2953, 2024.

[13] L. Yang, H. Yuan, J.-W. Peng, and C.-L. Zhang, "Performance modeling of air cycle heat pump water heater in cold climate," *Renewable Energy*, vol. 87, pp. 1067–1075, 2016, doi: 10.1016/j.renene.2015.08.055.

[14] B. Adler and R. Mauthner, "Rotation heat pump (RHP)," in *Proceedings of the 12th IEA Heat Pump Conference, Rotterdam, The Netherlands*, 2017, pp. 15–18.

[15] J. D. Kocher, "Thermodynamic and technoeconomic limitations of Brayton refrigeration for air conditioning," *International Journal of Refrigeration*, vol. 169, pp. 418–428, 2025, doi: 10.1016/j.ijrefrig.2024.11.013.

[16] L. Wang, H. Li, and J. Zhou, "Thermodynamic investigation of a centrifugal reverse Brayton cycle for refrigeration in air conditioning filed," *International Journal of Refrigeration*, vol. 152, pp. 176–191, 2023.

[17] L. Dai *et al.,* "A 2 kW-class free-piston Stirling heat pump prototype suitable for cold regions for domestic heating," *International Journal of Refrigeration*, vol. 159, pp. 112–123, 2024.

[18] G. Teng *et al.,* "Experimental study of an efficient low-temperature thermoacoustic Stirling heat pump," *International Journal of Refrigeration*, vol. 172, pp. 17–26, 2025, doi: 10.1016/j.ijrefrig.2025.01.005.

[19] X. Jin *et al.,* "Performance analysis of a two-stage vapor compression heat pump based on intercooling effect," *Case Studies in Thermal Engineering*, vol. 51, p. 103643, 2023.

[20] B. Luo and P. Zou, "Performance analysis of different single stage advanced vapor compression cycles and refrigerants for high temperature heat pumps," *International Journal of Refrigeration*, vol. 104, pp. 246–258, 2019.

[21] V. Venzik, "Experimentelle Untersuchung des Fluideinflusses auf die Thermodynamik der Wärmepumpe: Kohlenwasserstoffe und deren Gemische," Dissertation, Duisburg, Essen, Universität Duisburg-Essen, 2019, 2019.

[22] A. V. Olympios, J. Song, A. Ziolkowski, V. S. Shanmugam, and C. N. Markides, "Data-driven compressor performance maps and cost correlations for small-scale heat-pumping applications," *Energy*, vol. 291, p. 130171, 2024.

[23] A. Grauberger, D. Young, and T. Bandhauer, “Experimental validation of an organic rankine-vapor compression cooling cycle using low GWP refrigerant R1234ze (E),” *Applied Energy*, vol. 307, p. 118242, 2022.
[24] A. J. White, “Thermodynamic analysis of the reverse Joule - Brayton cycle heat pump for domestic heating,” *Applied Energy*, vol. 86, no. 11, pp. 2443–2450, 2009.
[25] N. Kabat, E. Jende, E. Nicke, and P. Stathopoulos, “Investigation on Process Architectures for High-Temperature Heat Pumps Based on a Reversed Brayton Cycle,” in *Turbo Expo: Power for Land, Sea, and Air*, 2023, V005T06A015.
[26] M. A. Yaqteen, Y. Chung, C. H. Song, and J. S. Kim, “Performance analysis of a high-temperature heat pump based on a cascaded reverse Brayton and vapor compression cycle,” *Energy Reports*, vol. 13, pp. 318–329, 2025.
[27] K. Thulukkanam, *Heat exchanger design handbook,* 2nd ed.: CRC press, 2013.
[28] O. Fawwaz Alrebei, A. Hamdan Al Assaf, M. S. Al-Kuwari, and A. Amhamed, “Lightweight methane-air gas turbine controller and simulator,” *Energy Conversion and Management: X*, vol. 15, p. 100242, 2022, doi: 10.1016/j.ecmx.2022.100242.
[29] Y. Song, X. Sun, and D. Huang, “Preliminary design and performance analysis of a centrifugal turbine for Organic Rankine Cycle (ORC) applications,” *Energy*, vol. 140, pp. 1239–1251, 2017, doi: 10.1016/j.energy.2017.08.061.
[30] A. P. Tran and P. Stathopoulos, “Dynamic simulation and experimental validation of a high-temperature Brayton heat pump,” *Applied Thermal Engineering*, p. 126536, 2025.
[31] F. Ahmed, H. Huang, S. Ahmed, and X. Wang, “A comprehensive review on modeling and performance optimization of Stirling engine,” *International Journal of Energy Research*, vol. 44, no. 8, pp. 6098–6127, 2020.
[32] J. E. Thorsen, H. Lund, and B. V. Mathiesen, “Progression of District Heating - 1st to 4th Generation,” Aalborg University, 2018. [Online]. Available: http://vbn.aau.dk/files/280710833/1_4GDH_progression_revised_May2018.pdf
[33] V. Muncan, I. Mujan, D. Macura, and A. S. Andelkovic, “The state of district heating and cooling in Europe - A literature-based assessment,” *Energy*, vol. 304, p. 132191, 2024, doi: 10.1016/j.energy.2024.132191.
[34] S. Buffa, M. Cozzini, M. D’antoni, M. Baratieri, and R. Fedrizzi, “5th generation district heating and cooling systems: A review of existing cases in Europe,” *Renewable and Sustainable Energy Reviews*, vol. 104, pp. 504–522, 2019.
[35] N. Fuchs, G. Yanez, B. Nkongdem, and J. Thomsen, “Evaluating low-temperature heat sources for large-scale heat pump integration: A method using open-source data and indicators,” *Applied Energy*, vol. 377, p. 124487, 2025.
[36] Joachim Ferstl, Niklas Wettberg, Michael Hinterstocker, and Andreas Möbius, “Wärmepumpen an Fließgewässern – Analyse des theoretischen Potenzials in Bayern,” Forschungsgesellschaft für Energiewirtschaft e.V. (FfE), München, 2024.
[37] Bayerisches Staatsministerium für Wirtschaft, Landesentwicklung und Energie, “Oberflächennahe Geothermie: Heizen und Kühlen mit Energie aus dem Untergrund,” Bayerisches Staatsministerium für Wirtschaft, Landesentwicklung und Energie (StMWi), 2021.
[38] M. P. Wilson and F. Worrall, “The heat recovery potential of ‘wastewater’: a national analysis of sewage effluent discharge temperatures,” *Environmental Science: Water Research & Technology*, vol. 7, no. 10, pp. 1760–1777, 2021.
[39] R. Lund and U. Persson, “Mapping of potential heat sources for heat pumps for district heating in Denmark,” *Energy*, vol. 110, pp. 129–138, 2016.
[40] *Application of high-power heat pumps*, VDI 4646, 2024.
[41] A. M. Whitman, *Thermodynamics: basic principles and engineering applications*: Springer, 2020.
[42] E. W. Lemmon, I. H. Bell, M. L. Huber, and M. O. McLinden, “NIST standard reference database 23: reference fluid thermodynamic and transport properties-REFPROP, Version 10.0, National Institute of Standards and Technology,” *Standard Reference Data Program, Gaithersburg*, pp. 45–46, 2018.
[43] Stoian Petrescu, Monica Costea, Michel Feidt, Ioan Ganea, and Nicolae Boriaru, Eds., *Advanced Thermodynamics of Irreversible Processes with Finite Speed and Finite Dimensions*. Calea Victoriei, nr. 118, 010093 Bucharest, Romania: AGIR Publishing House, 2015.
[44] M. H. Ahmadi, M. A. Ahmadi, A. H. Mohammadi, M. Feidt, and S. M. Pourkiaei, “Multi-objective optimization of an irreversible Stirling cryogenic refrigerator cycle,” *Energy Conversion and Management*, vol. 82, pp. 351–360, 2014, doi: 10.1016/j.enconman.2014.03.033.